

Barium Abundances in Cepheids

S.M. Andrievsky^{1,2,3*}, J.R.D. Lépine¹, S.A. Korotin², R.E. Luck⁴,
V.V. Kovtyukh², and W.J. Maciel¹

¹ *Instituto de Astronomia, Geofísica e Ciências Atmosféricas da Universidade de São Paulo, Cidade Universitária, CEP: 05508-900, São Paulo, SP, Brazil*

² *Department of Astronomy and Astronomical Observatory, Odessa National University, and Isaac Newton Institute of Chile Odessa branch Shevchenko Park, 65014 Odessa, Ukraine.*

³ *GEPI, Observatoire de Paris-Meudon, F-92125 Meudon Cedex, France,*

⁴ *Department of Astronomy, Case Western Reserve University, Cleveland, OH 44106.*

Accepted. Received ; in original form

ABSTRACT

We derived the barium atmospheric abundances for a large sample of Cepheids, comprising 270 stars. The sample covers a large range of galactocentric distances, from about 4 to 15 kpc, so that it is appropriated to investigate the existence of radial barium abundance gradients in the galactic disc. In fact, this is the first time that such a comprehensive analysis of the distribution of barium abundances in the galactic disc is carried out. As a result, we conclude that the Ba abundance distribution can be characterized by a zero gradient. This result is compared with derived gradients for other elements, and some reasons are briefly discussed for the independence of the barium abundances upon galactocentric distances.

Key words: stars: abundances – Galaxy: disc – Galaxy: evolution – stars: variables: Cepheids.

1 INTRODUCTION

In our extensive studies of the elemental distributions in the galactic disc based on studies of Cepheid spectra (Andrievsky et al. 2002a, Andrievsky et al. 2002b, Andrievsky et al. 2002c, Andrievsky et al. 2004, Luck et al. 2003, Luck et al. 2006, Luck et al. 2011, Luck & Lambert 2011), we have avoided the determination of barium abundances. Although three Ba II lines are available in the observed spectral domain, all are very strong in Cepheid spectra with equivalent widths ranging from 200 to 600 mÅ. A simple LTE analysis of such strong lines could produce incorrect abundance results due to NLTE effects in the atomic populations, and more importantly, due to strong saturation effects making the analysis particularly sensitive to the microturbulence.

The great majority of studies devoted to the barium abundance in the galactic disc are based on the LTE approximation, and most focus on nearby stars. Recently, a more sophisticated method: i.e., NLTE, has been applied to the galactic disc stars, but as in the case of older studies, only for those situated near the solar region (Korotin et al. 2010).

The present-day barium abundance distribution in galactic disc results from a variety of processes. The different processes include nucleosynthesis in AGB stars, supernovae of type II, as well as dynamical processes involving radial gas flows that lead to large scale mixing of the interstellar medium. The barium abundance distribution in the galactic disc (as well as distributions of the heavy r -/ $r + s$ -process elements like La, Ce and Nd) is necessary to constrain models of the Milky Way chemical evolution. Existing data on the barium content in objects situated at large distances from the Sun are scarce, and apparently insufficient to check the validity of model predictions (see, e.g. Figure 9 in Cescutti et al. 2007).

To investigate the barium abundances in distant stars we use the sample of Cepheids investigated in our previous works: Andrievsky et al. (2002a), Andrievsky et al. (2002b), Andrievsky et al. (2002c), Luck et al. (2003), Luck et al. (2006), Luck et al. (2011). In those papers, one can find information about the atmospheric parameters of the program stars and their spectra. For some stars, we have used the multi-phase observations described in Luck & Andrievsky (2004), Kovtyukh et al. (2005), Andrievsky et al. (2005), and Luck et al. (2008). The reasons for studying these stars are many. These stars are luminous, allowing them to serve as probes of distant regions. The methods of the abundance

* E-mail: scan@deneb1.odessa.ua

analysis of the stars of F-G spectral classes are well established; and finally, Cepheids are rather young stars, and thus they reflect the present-day characteristics of the galactic disc, even though they had time to migrate.

2 BARIUM ATOMIC MODEL AND METHOD OF ABUNDANCE DETERMINATION

Andrievsky et al. (2009) describe our model of barium atom in detail. Briefly, it consists of 31 levels of Ba I, 73 levels of Ba II, and the ground level of Ba III. Ninety-one bound-bound transitions between the first 28 levels of Ba II with $n < 12$ and $l < 5$ are computed in detail. The remaining levels are used for particle number conservation. For two levels, $5d^2D$ and $6p^2P_0$, fine structure was taken into account. Oscillator strengths, photoionization cross-sections, collisional rates, broadening parameters and test calculations are found in the above-mentioned paper.

Atomic level populations were determined using the MULTI code of Carlsson (1986) with modifications as given in Korotin et al. (1999). MULTI calculates the line profile for each line considered in detail. The line profile computed assuming either LTE or NLTE depends upon many parameters: the effective temperature of the model, the surface gravity, the microturbulent velocity, and the line damping as well as the populations in the appropriate levels. Departure coefficients, defined as the ratio of NLTE to LTE level populations, are also computed by MULTI, and they depend only on the model atom and model stellar atmosphere. Specifically, they are independent of the total abundance, the damping, and the microturbulence.

Barium atom has seven isotopes. Isotopic shifts are very small (about 2 mÅ). For two odd isotopes ^{135}Ba and ^{137}Ba the hyper-fine structure is quite important, and this produces additional complication in the line structure (several line components of the odd isotopes shifted relatively to the lines of even isotopes). This produces the shifts between the line components formed by odd and even isotopes. It is known that the most pronounced effect is seen in the Ba II line 4554.03 Å (out of our spectral region).

In principle, this effect has some influence on profile of the 6496.91 Å line. The components of the odd isotopes constitute two compact groups that are shifted on -4 and $+9$ mÅ relatively components of the even isotopes. For the rest of our two lines the corresponding shifts are too small to affect their line profiles.

As it was showed in the work of Mashonkina et al. (1999) for the adequate barium line modelling it is sufficient to use the three-component model suggested by Rutten (1978). For the calculations of the Ba line profiles in the spectra of young stars one can use the even-to-odd abundance ratio of 82:18 (Cameron 1982).

Since the equivalent widths of our program barium lines are larger than 250 mÅ, we can state that HFS does not have in this case any significant influence on the line profiles.

Three Ba II lines are available in our program spectra for the abundance analysis: 5853.68 Å, 6141.71 Å and 6496.91 Å. The barium abundance was derived by fitting calculated profiles to the observed profiles. All of the available barium lines are blended with lines of other elements.

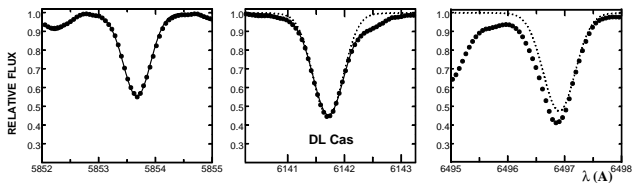


Figure 1. Profile fitting of the Ba II line in the DL Cas spectrum. Observed spectrum - dots, pure NLTE MULTI profile - dotted line, combined synthetic spectrum - smooth line.

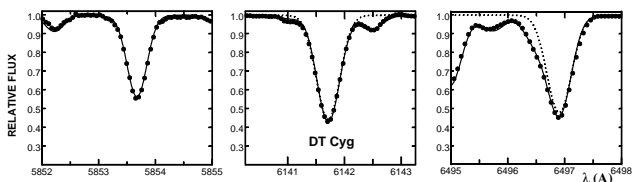


Figure 2. The same as Figure 1 but for DT Cyg.

(iron lines, in particular). The blending effect is more significant for the 6141.71 and 6496.91 Å lines (for 5853.68 Å line this effect is negligible). Proper comparison of the observed and computed profiles thus requires a multi-element synthesis. For this process, we fold the NLTE (MULTI) calculations into the LTE synthetic spectrum code SYNTHV (Tsymbol 1996). With these programs, we calculated synthetic spectra for each Ba II line region taking into account all the lines in each region listed in the VALD database (<http://ams.astro.univie.ac.at/vald/>). For the barium lines, the corresponding departure coefficients (so-called b -factors: $b = n_i/n_i^*$ - the ratio of NLTE-to-LTE level populations) are input to SYNTHV, where they are used in the calculation of the line source function and barium line profiles. Figures 1 and 2 show the quality of fit achieved by this process.

In Fig. 3 we show how blending lines together with Ba II lines form the resulting profile of 6141.71 and 6496.91 Å lines (an example for Cepheid DL Cas). We can see that the contribution from the blending lines (Fe I 6141.732 Å for 6141.71 Å, and Fe I 6496.467 Å for 6496.91 Å) is not extremely large (we have also to note that there are also two weak lines in the wings of 6141.71 Å line - Fe II 6141.033 Å and Si I 6142.483 Å). If spectral synthesis is properly done, then this contribution is adequately accounted. For blending lines we used the reliable atomic data from the VALDatabase, see the reference above, while abundances of elements producing those lines are taken from the series of our previous papers, i.e. they were fixed. In particular, in this case VALD data are based on original data from Fuhr & Wiese (2006). In fact, we always relied more on the barium abundance derived from 5853.68 Å line. In a few cases this line was not available in our spectra, or its profile was spoiled due to some reasons. In those cases, only the rest two lines were used in abundance analysis. As a rule, the barium abundance derived from 5853.68 Å line and from other two lines agreed well between themselves. If there was a significant deviation of the barium abundance from one of the 6141.71 and 6496.91 Å lines, the corresponding line was not considered in the final statistics.

Stellar parameters for all stars were taken from our

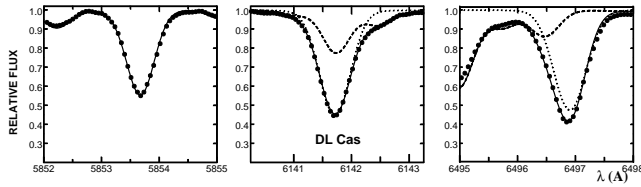


Figure 3. Ba II lines, blending lines and resulting profiles in DL Cas spectrum. Dots - observed spectrum, smooth line - combined calculated profile, dotted line - pure Ba II line profile, dashed line - blending spectral line.

previous works (for a compendium, see Luck et al. 2011). These parameters were determined from a combined LTE excitation and ionization balance analysis. In particular, the microturbulent velocity depends solely on Fe II lines. In our syntheses, we used previously published (see Luck et al. 2011) abundances of elements whose lines were treated in SYNTHV: i.e., blending lines and lines situated in the vicinity of barium lines.

In some cases, our program Cepheids exhibit asymmetric line profiles due to dynamic phenomena associated with pulsation. In such cases, our profile fitting cannot be applied, and thus, spectra with greatly asymmetric lines were excluded from the analysis. A few exceptions were allowed in which we used the 5853.68 Å line alone to derive NLTE barium abundance. This line is not heavily blended, and its equivalent width is measurable by direct integration.

3 RESULTS OF THE NLTE BARIUM ABUNDANCE DETERMINATION AND SOURCES OF ABUNDANCE ERRORS

Table 3 contains the list of program stars, phases for the selected spectra, adopted atmosphere parameters, galactocentric distances (based on $R_{\text{Sun}} = 7.9$ kpc), NLTE barium abundances, sigma values and the number of analyzed barium line profiles. In some cases, adjacent echelle orders contain the same barium lines and each profile was analyzed independently. For some stars we have multiphase observations, therefore the number of analyzed barium line profiles is the number of available spectra multiplied by the number of available barium lines in each spectrum (this number is listed in Table 3).

We have investigated the parameter sensitivity of the derived Ba abundance. Our initial parameters were $T_{\text{eff}} = 6000$ K, $\log g = 2.0$, $V_t = 4.0$ km s⁻¹ with $[\text{Fe}/\text{H}] = 0$. We then generated lines assuming $\log \epsilon(\text{Ba}) = 2.17$ and matched them using parameter sets that vary one parameter at a time. An increase of 150 K in effective temperature changes the Ba abundance by +0.1 dex, a 0.2 dex increase in $\log g$ gives a change of +0.06, and a microturbulent velocity increase and decrease of 0.5 km s⁻¹ yields a decrease and increase in abundance of -0.23 and +0.28 dex respectively. The formal parameter related uncertainty is thus about ± 0.3 dex. However, note that at lower microturbulent velocities the dependence of the barium abundance on V_t is much stronger.

In Figures 4 through 8 we show the derived barium abundances as a function of the pulsation phase, effective

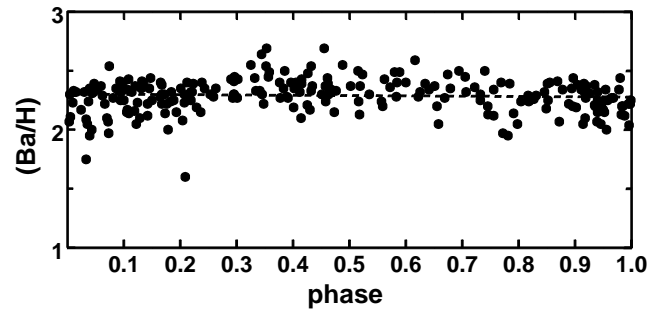


Figure 4. Barium abundance vs. phase for program stars spectra. Combined plot.

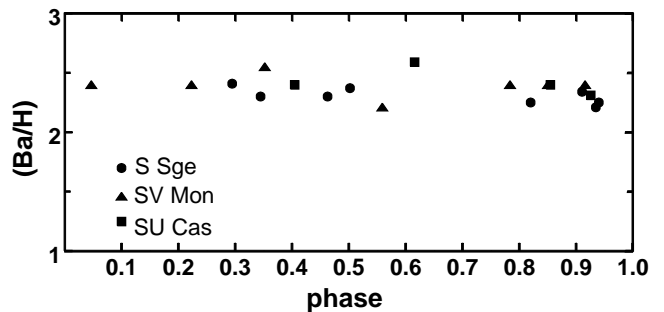


Figure 5. Barium abundance vs. phase for program stars spectra with multiphase observations.

temperature, surface gravity, and microturbulent velocity. As one can see, there is no significant dependence on phase ϕ (for three stars where we used multiphase observations Figure 5 shows such a dependence), T_{eff} , or $\log g$, but there is a quite clear variation with microturbulent velocity (Figure 8). This relation is quite disconcerting as it means that we are dealing with strong saturation in the lines, and hence, the dramatic dependence of abundance on assumed microturbulent velocity. To illustrate, we give in Table 1 the dependence of the Ba abundance on microturbulent velocity for UX Car.

In the case of UX Car (Table 1), the Fe II derived V_t (4.7 km s⁻¹) yields excellent agreement between the three Ba II lines. This is not surprising as this V_t is in the region of V_t versus Ba (see Figure 8) where there is no obvious dependence between abundance and V_t . This suggests that it might be possible to find the proper V_t value for Ba II by forcing the three lines to yield the same Ba abundance

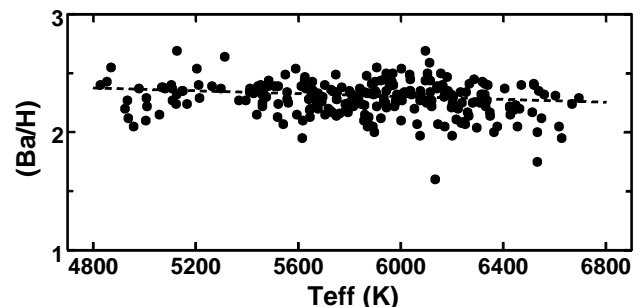


Figure 6. Barium abundance vs. effective temperature.

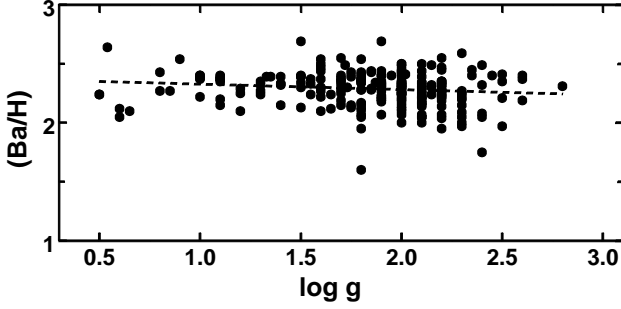


Figure 7. Same as Figure 6, but for surface gravity.

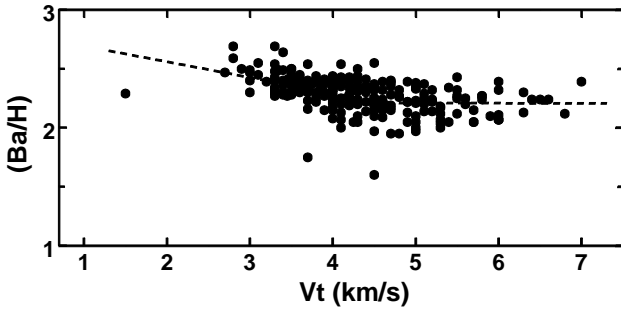


Figure 8. Same as Figure 6, but for microturbulent velocity.

using V_t as a free parameter. The result of this approach for IR Cep is shown in Table 2. The idea behind this attempt is that each Ba II feature has a constant contribution from Ba that is defined by the best fitting synthesis. One then uses the best fitting abundance to the profile to calculate the unblended Ba equivalent width. One then matches the equivalent width for each selected microturbulent velocity. In this test, we have matched the equivalent widths using an LTE approach. As the primary problem we are trying to overcome now is not level populations but saturation effects. While there is a range of equivalent widths in the Ba II lines, all lines are saturated and it is not possible to obtain a clear-cut indication of a better value to use for V_t . In this case, the Fe II V_t is 2.9 km s^{-1} , which gives a spread of about 0.13 dex between the Ba II lines. The spread at 4.0 km s^{-1} is marginally better at 0.10 dex, but given the overall uncertainties, does not significantly improve the confidence level of the abundance determination. It is also of interest that above about 6 km s^{-1} the lines become only weakly dependent on V_t ; that is, they are de-saturated and behave as weak-lines. Also included in Table 2 is the best fitting Ba abundance for the NLTE analysis. The NLTE corrections for these lines are not especially large averaging around -0.1 dex.

Table 1. NLTE abundances for UX Car

Line	$V_t, \text{ km s}^{-1}$			
	3.5	4.0	4.7	5.3
5853	2.58	2.37	2.19	2.09
6141	2.84	2.53	2.19	1.99
6496	2.81	2.50	2.19	2.01

The origin of the dependence of the Ba abundance of V_t as shown in Figure 8 could arise in a velocity stratification in the atmosphere of Cepheids. The solar atmosphere exhibits an increasing microturbulent velocity with height (Stodilka & Malynch 2006) and it would not be surprising if similar temperature but higher luminosity objects showed the same phenomena. Quite strong barium lines have effective depth of formation high in the atmosphere, while weaker (on average) iron lines used for microturbulence determination must be formed deeper in atmosphere at a lower V_t .

Since there is no straightforward method to account for the dependence seen in Figure 8, we simply divide the barium abundance data into two parts based on the microturbulent velocity. From Figure 8, one can estimate that the break in the (Ba/H) - V_t relation roughly corresponds to $V_t = 3.8 \text{ km s}^{-1}$.

4 THE BARIUM RADIAL ABUNDANCE DISTRIBUTION

Our primary interest in previous Cepheid abundance studies has been the distribution of the elements in the galactic disc, and the motivation for this study of Ba abundances is no exception. While there is uncertainty about the abundances themselves, we shall persevere and consider the abundance distribution found from our Ba data.

In Figure 9 we show the radial barium abundance distribution in galactic disc as derived from the total sample of the stars and from the sample with $V_t > 3.8 \text{ km s}^{-1}$ (the distances are given in Table 3). With the exception of a few deviant stars (such as EE Mon at $R_G = 15 \text{ kpc}$) the barium abundance distribution looks essentially flat. The mean value for the total sample is $\langle \text{Ba}/\text{H} \rangle = 2.29 \pm 0.15$. If we use barium abundance data for the part of the sample with $V_t > 3.8 \text{ km s}^{-1}$, the mean value is $\langle \text{Ba}/\text{H} \rangle = 2.25 \pm 0.13$. Both values are the same within the estimated errors. What is important to note is that in both cases we have almost zero gradient.

5 DISCUSSION

As a first approach to the Ba gradient, a linear regression was fitted to the data of Figures 9, with the formal result being: $(\text{Ba}/\text{H}) = +0.0066 R_G + 2.2345$ (the total sample), and $(\text{Ba}/\text{H}) = +0.0003 R_G + 2.2456$ ($V_t > 3.8 \text{ km s}^{-1}$). From this, we conclude:

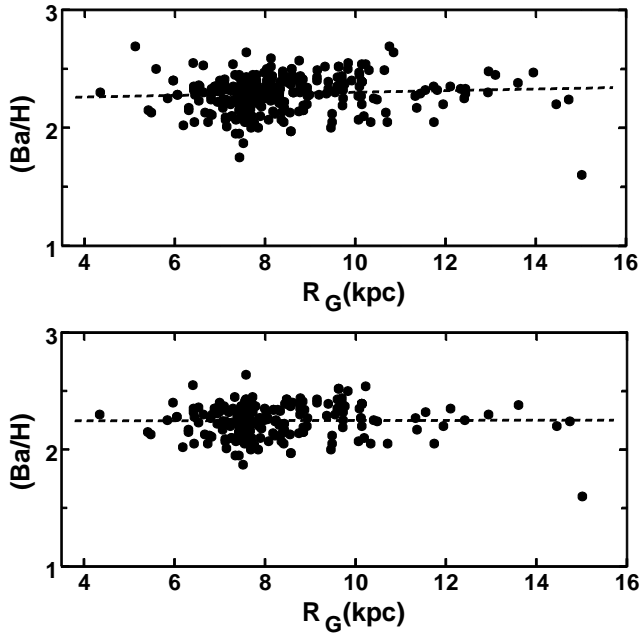
1) Barium abundances appear to be the same with a quite large scatter around the mean in the region spanning galactocentric distances from 4 to 15 kpc.

2) The mean (Ba/H) value for the solar neighborhood is near the solar barium abundance. The Cepheid mean values are 2.29 for the total sample and 2.25 for the stars with $V_t > 3.8 \text{ km s}^{-1}$ versus a solar (NLTE) barium abundance of 2.17.

What could be the origin of a homogeneous distribution of barium in the galactic radius? Let us consider the iron distribution in the disc presented in Figure 10 (data from Luck et al. 2011). This figure shows that the mean iron abundance in the range of galactocentric distances from 9 to

Table 2. Abundances for IR Cep

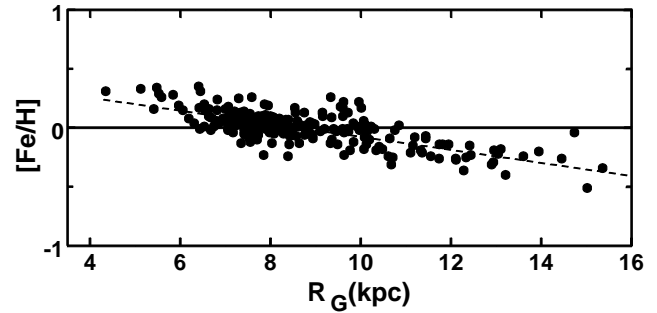
		V _t , km s ⁻¹								
Line	EW, mÅ	2.0	2.5	3.0	3.5	4.0	4.5	5.0	6.0	7.0
LTE										
5853	196	3.23	2.81	2.46	2.18	1.97	1.83	1.73	1.58	1.50
6141	270	3.17	2.89	2.54	2.22	1.94	1.72	1.53	1.26	1.09
6496	280	3.30	2.96	2.59	2.29	2.04	1.83	1.67	1.43	1.28
NLTE			2.75		2.08					

**Figure 9.** (Ba/H) data vs. galactocentric distance. Upper plot - the total sample of stars, lower plot - part of the sample with $V_t > 3.8$ km s⁻¹.

14 kpc is about 0.2 dex lower than in the solar vicinity. This difference would be about 0.3 dex if we adopt the metallicity distribution with a step at corotation as proposed by Lépine et al. (2011) based on a study of open clusters. One could expect to detect lower barium abundance in the region 9-14 kpc relative to the solar value, but this is not the case, as one can see in Figure 9.

If one adopts for lanthanum, praseodymium, neodymium, samarium, and europium the main s - and r -process dissection provided by Simmerer et al. (2004), and plot their r -process fractions vs. abundance gradients derived for these elements by Luck & Lambert (2011), then one can note the slight (and quite loose) slope in the "abundance gradient - r -process fraction" dependence. Using this dependence together with barium r -process fraction 0.15, one can derive the expected barium abundance gradient of about -0.03 dex/kpc, which is in contrast to the zero slope from the present paper.

This discrepancy between observed and expected abundance gradient for Ba abundance requires either a peculiar s -process pattern with lower " r "-process fraction for all above considered elements, or there is a systematic error in the Ba

**Figure 10.** [Fe/H] vs. galactocentric distance from Luck & Lambert (2011) - Figure 1.

abundance analysis, an odd error that is not revealed by the temperature, gravity, or phase-dependent spectra.

Another possibility could be connected to some unaccounted yet effect, which may be hidden in the literature La, Ce, Nd and Eu LTE abundance data derived for Cepheids, and respective gradients based on them. For instance, the NLTE deviations for these elements may be different for the stars with (even slightly) different metallicities located at the different galactocentric distances.

Since there are no other literature large studies of the barium abundance distributions in the disc, and thus there is no possibility to compare our barium data with the results of other specialists, we prefer to leave a detailed discussion of this problem for the future time, until the new observational and theoretical data on barium and other heavy s -process element distributions in the galactic disc appear.

ACKNOWLEDGMENTS

SMA kindly acknowledges the Universidade de São Paulo (USP) and Instituto de Astronomia, Geofísica e Ciências Atmosféricas da USP for support and hospitality during his stay in Brasil. SAK thanks the SCOPES grant No. IZ73Z0-128180/1 for partial financial support.

Authors thank anonymous referee for his/her comments.

REFERENCES

Andrievsky S.M., Kovtyukh V.V., Luck R.E., Lépine J.R.D., Bersier D., Maciel W.J., Barbuy B., Klochkova

- V.G., Panchuk V.E., Karpishek R.U., 2002a, A&A 381, 32
- Andrievsky S.M., Bersier D., Kovtyukh V.V., Luck R.E., Maciel W.J., Lépine J.R.D., Beletsky Yu.V., 2002b, A&A 384, 140
- Andrievsky S.M., Kovtyukh V.V., Luck R.E., Lépine J.R.D., Maciel W.J., Beletsky Yu.V., 2002c, A&A 392, 491
- Andrievsky S.M., Luck R.E., Kovtyukh V.V., 2005, AJ 130, 1880.
- Andrievsky S.M., Luck R.E., Martin P., Lépine J.R.D., 2004, A&A 413, 159
- Andrievsky S.M., Spite M., Korotin S.A., Spite F., Francois P., Bonifacio P., Cayrel R., Hill V., 2009, A&A 494, 1083
- Cameron A.G.W., 1982, ApSS 82, 123
- Carlsson M., 1986, Uppsala Obs. Rep. 33
- Cescutti G., Matteucci F., Francois P., Chiappini C., 2007, A&A 462, 943
- Fuhr J.R. & Wiese W.L., 2006, J. Phys. Chem. Ref. Data 35, 1669.
- Korotin S.A., Andrievsky S.M., Luck R.E., 1999, A&A 351, 168
- Korotin S., Mishenina T., Gorbaneva T., Soubiran C., 2010, Proceedings of the 11th Symposium on Nuclei in the Cosmos. 19-23 July 2010. Heidelberg, Germany
- Kovtyukh, V.V., Andrievsky S.M., Belik S.I., Luck R.E., 2005, AJ 129, 433
- Lépine J.R.D., Cruz P., Scarano S., Jr., Barros D.A., Dias W.S., Pompeia L., Andrievsky S.M., Carraro G., Famaey B., 2011, MNRAS 417, 698
- Luck R.E., Andrievsky S.M., 2004, AJ 128, 343
- Luck, R.E., Andrievsky S.M., Fokin, A. & Kovtyukh V.V., 2008, AJ 136, 98.
- Luck R.E., Andrievsky S.M., Kovtyukh V.V., Gieren W., Graczyk D., 2011, AJ 142, 51L
- Luck R.E., Gieren W.P., Andrievsky S.M., Kovtyukh V.V., Fouqué P., Pont F., Kienzle F., 2003, A&A 401, 939
- Luck R.E., Kovtyukh V.V., Andrievsky S.M., 2006, AJ 132, 902
- Luck R.E., Lambert, D.L., 2011, AJ 142, 137L
- Mashonkina L., Gehren T., Bikmaev I., 1999, A&A 343, 519
- Rutten R.J., 1978, Solar Phys. 56, 237
- Simmerer J., Sneden Ch., Cowan J.J. et al., 2004, ApJ 617, 1091
- Stodilka, M.I., Malynch, S.Z., 2006, MNRAS 373, 1523
- Tsymbal V.V., 1996, Model Atmospheres and Spectrum Synthesis, ed. S.J. Adelman, F. Kupka, W.W. Weiss (San Francisco), ASP Conf. Ser., 108

Table 3. Program stars, their phase parameters and barium abundance

Star	phase	T _{eff} , K	log <i>g</i>	V _t , km s ⁻¹	[Fe/H]	R _G , (kpc)	log $\epsilon(\text{Ba})_{\text{NLTE}}$	$\sigma(\text{Ba})$	N lines
AA Gem	0.625	5126	1.40	4.40	-0.24	11.550	2.32	0.18	2
AA Mon	0.106	6261	2.10	4.00	-0.21	11.364	2.17	0.12	3
AC Mon	0.081	6075	1.90	4.80	-0.22	10.121	2.27	0.12	3
AC Mon	0.919	6121	2.20	5.80	-0.07	10.121	2.27	0.12	3
AD Cru	0.030	6000	2.00	4.00	0.06	6.987	2.32	0.13	3
AD Gem	0.818	5784	2.15	4.30	-0.19	10.481	2.24	0.18	2
AE Tau	0.377	5981	2.30	4.00	-0.19	11.326	2.27	0.13	3
AE Vel	0.732	5460	1.70	4.50	0.05	7.983	2.25	0.20	3
AG Cru	0.039	6628	2.20	4.70	-0.13	7.346	1.95	0.13	3
AH Vel	0.383	6037	2.20	4.30	0.10	7.996	2.35	0.13	3
AO Aur	0.707	5459	1.70	3.60	-0.14	11.813	2.32	0.18	2
AP Pup	0.052	6233	2.10	4.20	0.06	8.189	2.34	0.13	3
AP Sgr	0.093	6328	2.02	3.46	0.10	7.101	2.41	0.15	6
AQ Car	0.998	5815	1.90	4.90	0.06	7.631	2.22	0.13	3
AQ Pup	0.756	4937	0.60	5.50	-0.14	9.487	2.12	0.13	3
AQ Pup	0.798	4958	0.60	5.70	-0.14	9.487	2.05	0.15	3
AS Per	0.580	5550	1.72	3.35	0.10	9.154	2.49	0.15	5
AT Pup	0.658	6455	2.10	5.00	-0.14	8.412	2.05	0.15	3
AV Cir	0.207	6169	2.10	3.30	0.10	7.516	2.30	0.13	3
AV Sgr	0.982	5875	1.75	4.90	0.34	5.475	2.13	0.15	3
AW Per	0.295	5989	1.90	3.60	0.00	8.622	2.30	0.13	5
AW Per	0.451	5836	2.00	3.70	0.00	8.622	2.30	0.13	6
AX Cir	0.119	5761	1.80	3.70	-0.05	7.530	2.16	0.13	3
AX Cir	0.745	5648	1.90	4.50	-0.07	7.530	2.20	0.12	3
AY Cen	0.999	5933	2.10	4.50	0.01	7.424	2.25	0.10	3
AZ Cen	0.947	6425	2.30	4.00	-0.05	7.413	2.21	0.10	3
BB Cen	0.183	6202	2.30	4.60	0.13	7.126	2.24	0.13	3
BB Gem	0.589	6035	2.40	3.00	-0.09	10.641	2.49	0.18	2
BB Her	0.259	5750	1.80	4.20	0.16	6.054	2.28	0.13	6
BB Her	0.389	5556	1.70	4.20	0.13	6.054	2.28	0.14	6
BB Sgr	0.878	5859	1.87	4.47	0.08	7.138	2.34	0.17	5
BC Pup	0.062	6695	2.00	3.50	-0.20	12.440	2.29	0.13	3
BC Pup	0.341	5879	1.90	3.30	-0.24	12.440	2.33	0.14	3
BD Cas	0.772	6200	2.50	5.00	-0.07	8.574	1.97	0.18	3
BD Cas	0.073	6075	2.30	4.50	-0.07	8.574	1.97	0.17	3
β Dor	0.128	5618	1.60	4.30	-0.01	7.896	2.10	0.13	6
BF Oph	0.033	6246	2.30	4.60	0.05	7.121	2.09	0.10	3
BF Oph		5541	1.90	4.10	-0.01	7.121	2.07	0.11	3
BG Cru	0.150	6309	2.30	4.20	0.06	7.694	2.25	0.16	3
BG Cru	0.188	6101	2.00	3.80	-0.02	7.694	2.25	0.15	6
BG Lac	0.147	5923	1.90	3.80	0.01	8.158	2.44	0.13	5
BG Lac	0.332	5625	1.85	3.60	0.02	8.158	2.44	0.13	6
BG Vel	0.849	5727	1.90	5.30	-0.01	7.922	2.18	0.13	3
BM Per	0.344	5313	0.54	3.40	0.10	10.851	2.64	0.18	5
BN Pup	0.396	5105	1.00	3.50	0.01	9.920	2.40	0.15	3
BP Cir	0.033	6533	2.40	3.70	-0.06	7.431	1.75	0.15	3
CD Cyg	0.376	5211	1.00	3.50	0.10	7.474	2.40	0.13	6
CD Cyg	0.434	5108	1.10	4.00	0.15	7.474	2.37	0.14	6
CD Cyg	0.519	4979	1.00	4.00	0.08	7.474	2.37	0.13	6
CE Cas A	0.732	5817	1.73	3.81	0.18	9.549	2.30	0.20	5
CE Pup	0.804	5846	1.30	5.80	-0.04	14.739	2.24	0.13	3
CF Cas	0.584	5454	1.70	4.30	0.01	9.702	2.40	0.15	6
CF Cas	0.980	6115	2.00	4.00	-0.03	9.702	2.44	0.16	6
CF Cas	0.238	5704	1.90	3.70	0.02	9.702	2.40	0.15	6
CH Cas	0.108	6319	1.80	5.50	-0.08	9.601	2.43	0.17	5
CN Car	0.066	6331	2.20	4.30	0.06	7.802	2.22	0.13	3
CP Cep	0.243	5150	1.30	4.10	-0.14	9.600	2.35	0.17	3
CR Cep	0.634	5443	1.33	4.02	-0.06	8.442	2.39	0.15	6
CS Ori	0.679	6539	2.50	3.60	-0.26	11.738	2.35	0.15	3
CU Mon	0.655	5677	1.90	4.50	-0.25	14.451	2.20	0.15	3
CV Mon	0.178	5897	2.00	4.10	-0.03	9.461	2.00	0.15	3
CX Vel	0.003	6251	2.20	5.30	0.06	8.360	2.07	0.13	3
CY Car	0.095	6042	2.20	4.00	0.10	7.471	2.32	0.13	3
CY Cas	0.391	5369	0.85	3.45	0.06	10.062	2.27	0.18	5

Table 3 – *continued*

Star	phase	T _{eff} , K	log <i>g</i>	V _t , km s ⁻¹	[Fe/H]	R _G , (kpc)	log $\epsilon(\text{Ba})_{\text{NLTE}}$	$\sigma(\text{Ba})$	N lines
DD Cas	0.039	5901	1.80	4.50	0.04	9.602	2.35	0.18	5
DF Cas	0.401	5644	2.20	4.65	0.13	9.718	2.19	0.18	3
DK Vel	0.009	6448	2.20	3.70	-0.02	8.126	2.23	0.13	3
DL Cas	0.105	5860	1.70	4.70	-0.01	8.846	2.15	0.13	6
DL Cas	0.229	5786	1.70	4.20	-0.01	8.846	2.19	0.13	6
DL Cas	0.473	5438	1.40	4.00	-0.01	8.846	2.15	0.14	6
DR Vel	0.165	5482	1.50	3.80	0.08	8.036	2.40	0.13	3
DT Cyg	0.651	6406	2.60	3.70	0.16	7.805	2.37	0.13	6
DT Cyg	0.705	6286	2.35	3.10	0.10	7.805	2.45	0.13	6
DT Cyg	0.769	6339	2.45	3.40	0.13	7.805	2.40	0.13	6
DX Gem	0.353	6096	1.90	2.80	-0.02	10.755	2.69	0.20	2
DY Car	0.956	6533	2.30	5.30	-0.07	7.686	2.00	0.13	3
EE Mon	0.209	6134	1.80	4.50	-0.51	15.018	1.60	0.18	3
EK Mon	0.918	6001	2.00	4.50	-0.10	10.191	2.10	0.20	3
ER Car	0.872	5874	2.10	6.00	0.03	7.597	2.07	0.13	3
η Aql	0.263	5800	1.90	4.00	0.09	7.713	2.35	0.13	6
η Aql	0.404	5612	1.75	3.90	0.10	7.713	2.39	0.13	6
η Aql	0.462	5508	1.80	4.00	0.08	7.713	2.39	0.13	6
EU Tau	0.172	6203	2.00	3.00	-0.06	8.933	2.30	0.13	6
EU Tau	0.641	6014	2.20	3.30	-0.06	8.933	2.34	0.13	6
EW Sct	0.572	5655	1.70	3.40	0.04	7.568	2.36	0.13	6
EW Sct	0.722	5728	1.80	3.50	0.04	7.568	2.36	0.13	6
EX Vel	0.954	5902	2.00	5.00	0.05	8.872	2.34	0.13	3
FF Aql	0.219	6172	2.15	4.30	0.00	7.629	2.32	0.18	6
FF Aql	0.846	6328	2.10	5.20	0.09	7.629	2.32	0.17	6
FF Aql	0.995	6425	2.10	4.90	0.02	7.629	2.22	0.18	6
FG Mon	0.523	5626	1.60	3.00	-0.20	13.944	2.47	0.15	3
FG Vel	0.756	5411	1.50	4.40	-0.05	8.286	2.34	0.18	3
FI Car	0.215	5215	1.20	3.80	-0.01	8.107	2.29	0.13	6
FI Mon	0.356	5938	2.00	3.50	-0.18	13.106	2.45	0.15	6
FM Aql	0.432	5590	1.60	3.70	0.06	7.290	2.54	0.15	6
FM Cas	0.669	5395	1.60	4.20	-0.12	8.941	2.27	0.15	5
FN Vel	0.221	5809	1.90	3.70	0.06	7.850	2.32	0.15	3
FR Car	0.011	5905	2.00	5.00	0.02	7.387	2.33	0.13	6
GH Car	0.965	6336	2.00	5.50	-0.01	7.414	2.27	0.13	3
GH Lup	0.142	5460	1.60	4.60	0.08	6.944	2.22	0.13	3
GQ Ori	0.074	6002	1.80	4.10	0.01	10.226	2.54	0.18	5
GU Nor	0.145	6036	2.20	3.60	0.15	6.553	2.35	0.13	3
GX Car	0.996	6297	2.20	5.30	0.01	7.762	2.04	0.13	3
HW Car	0.947	5671	2.00	5.20	0.04	7.556	2.24	0.13	3
HW Pup	0.432	5869	1.55	3.60	-0.15	12.332	2.33	0.15	3
IO Car	0.072	6145	1.80	6.00	-0.05	8.078	2.07	0.15	3
IR Cep	0.385	6104	2.10	2.90	0.11	8.037	2.50	0.15	6
IT Car	0.950	5794	1.80	4.70	0.06	7.451	2.17	0.13	3
KK Cen	0.012	5894	1.90	5.50	0.12	7.542	2.32	0.13	3
KN Cen	0.488	4870	1.70	4.50	0.35	6.404	2.55	0.18	3
KQ Sco	0.940	5058	1.10	5.70	0.16	5.409	2.15	0.17	3
L Car	0.094	5298	1.10	4.50	0.05	7.794	2.37	0.15	3
LR TrA	0.086	5943	2.20	4.40	0.25	7.291	2.35	0.13	3
MM Per	0.358	5746	2.15	3.40	-0.01	10.304	2.49	0.18	2
MW Cyg	0.458	5522	1.65	4.00	0.05	7.553	2.24	0.15	5
MY Pup	0.114	6317	2.20	4.80	-0.14	8.028	2.32	0.13	3
MZ Cen	0.207	5816	1.90	5.20	0.20	6.531	2.23	0.15	3
NT Pup	0.219	5561	1.20	4.00	-0.15	12.416	2.25	0.13	3
QY Cen	0.004	6205	2.00	6.30	0.16	6.638	2.30	0.20	1
R Cru	0.100	6203	2.00	4.00	0.08	7.539	2.25	0.13	3
R Mus	0.184	5985	2.00	4.00	0.10	7.502	2.32	0.13	3
R TrA	0.167	6121	2.20	3.80	0.06	7.475	2.22	0.13	3
RR Lac	0.518	5646	1.80	4.10	0.00	8.554	2.13	0.15	5
RS Ori	0.831	5934	1.85	5.10	-0.02	9.363	2.29	0.15	3
RS Pup	0.905	5068	1.00	5.00	0.20	8.540	2.38	0.13	3
RS Pup	0.935	5073	1.00	4.70	0.16	8.540	2.38	0.13	3
RT Aur	0.535	5696	2.15	3.30	0.05	8.304	2.30	0.13	6
RT Aur	0.583	5686	1.85	3.40	0.07	8.304	2.28	0.14	6

Table 3 – *continued*

Star	phase	T _{eff} , K	log <i>g</i>	V _t , km s ⁻¹	[Fe/H]	R _G , (kpc)	log $\epsilon(\text{Ba})_{\text{NLTE}}$	$\sigma(\text{Ba})$	N lines
RT Mus	0.204	6236	2.40	4.00	0.02	7.426	2.08	0.13	3
RV Sco	0.914	6172	2.30	5.40	0.03	6.734	2.05	0.13	3
RX Aur	0.135	6165	2.00	4.70	0.04	9.397	2.39	0.15	3
RX Aur	0.334	5677	1.40	3.70	-0.06	9.397	2.33	0.14	3
RX Cam	0.212	5971	1.95	4.10	0.07	8.614	2.40	0.15	6
RX Cam	0.461	5485	1.60	3.50	0.05	8.614	2.44	0.14	6
RY CMa	0.897	6096	2.10	4.30	0.02	8.781	2.44	0.20	2
RY Sco	0.746	5519	1.50	6.30	0.04	6.668	2.13	0.20	6
RY Vel	0.412	5466	1.30	4.60	0.10	7.731	2.32	0.13	3
RZ Gem	0.325	5906	2.20	3.10	-0.12	9.838	2.55	0.20	2
RZ Vel	0.037	6669	1.55	6.50	-0.03	8.225	2.24	0.15	3
RZ Vel	0.988	6549	1.65	6.80	-0.11	8.225	2.12	0.14	3
S Cru	0.983	6464	2.10	4.10	-0.12	7.553	2.20	0.13	3
S Mus	0.106	5752	1.80	4.40	-0.02	7.564	2.34	0.13	3
S Nor	0.124	5859	2.00	5.00	0.07	7.169	2.23	0.13	3
S Sge	0.295	5887	1.80	3.90	0.10	7.552	2.41	0.18	3
S Sge	0.345	5661	1.90	4.40	0.10	7.552	2.30	0.17	3
S Sge	0.463	5476	1.60	3.90	0.10	7.552	2.30	0.16	3
S Sge	0.502	5412	1.55	3.75	0.10	7.552	2.37	0.18	3
S Sge	0.820	5799	2.10	5.50	0.10	7.552	2.25	0.19	3
S Sge	0.911	6115	2.00	5.00	0.07	7.552	2.34	0.17	3
S Sge	0.935	6198	2.10	5.00	0.08	7.552	2.21	0.16	3
S Sge	0.940	6239	2.20	4.10	0.10	7.552	2.25	0.17	3
S TrA	0.176	5976	2.10	4.20	0.12	7.283	2.22	0.13	3
S Vul	0.516	5166	0.50	6.40	-0.04	7.067	2.24	0.18	6
S Vul	0.557	5123	0.50	6.60	-0.01	7.067	2.24	0.17	6
ST Tau	0.132	6268	2.00	3.50		8.834	2.41	0.15	6
ST Tau	0.869	6519	2.50	4.40		8.834	2.41	0.16	6
ST Vel	0.978	6255	2.10	4.30	0.00	8.183	2.34	0.13	3
SU Cas	0.405	6162	2.35	3.00	0.08	8.127	2.40	0.15	6
SU Cas	0.616	6112	2.30	2.80	0.06	8.127	2.59	0.14	6
SU Cas	0.855	6520	2.60	3.30	0.06	8.127	2.40	0.15	6
SU Cas	0.926	6603	2.80	3.50	0.02	8.127	2.31	0.15	6
SU Cyg	0.415	5956	2.10	3.20	0.00	7.603	2.39	0.17	6
SU Cyg	0.917	6197	2.20	4.25	-0.03	7.603	2.32	0.18	6
SU Cyg	0.940	6314	2.40	4.50	-0.03	7.603	2.32	0.18	6
SV Mon	0.047	6141	1.50	4.60	-0.05	10.143	2.39	0.18	5
SV Mon	0.223	5464	1.10	4.20	0.06	10.143	2.39	0.15	6
SV Mon	0.352	5204	0.90	3.30	-0.01	10.143	2.54	0.17	6
SV Mon	0.559	4924	1.10	4.50	0.00	10.143	2.20	0.17	3
SV Mon	0.784	5263	1.35	7.00	-0.07	10.143	2.39	0.18	6
SV Mon	0.851	5522	1.50	6.00	-0.05	10.143	2.39	0.17	6
SV Mon	0.916	5482	1.40	4.90	-0.04	10.143	2.39	0.18	6
SV Per	0.894	5734	1.70	4.30	-0.05	10.088	2.35	0.15	5
SV Vel	0.939	6064	2.00	6.00	0.08	7.594	2.07	0.15	3
SV Vul	0.070	5856	1.20	5.90	0.11	7.261	2.10	0.13	6
SV Vul	0.414	5005	0.65	5.00	-0.01	7.261	2.10	0.14	6
SW Cas	0.791	5749	2.00	5.10	0.02	8.747	2.14	0.20	2
SW Vel	0.348	5010	1.00	4.40	0.00	8.427	2.22	0.15	3
SX Car	0.943	6513	2.10	4.50	-0.09	7.586	2.17	0.13	3
SX Vel	0.852	6280	2.00	4.50	0.00	8.245	2.25	0.13	3
SY Cas	0.985	5718	2.00	4.30	-0.06	8.928	2.20	0.15	6
SY Nor	0.164	5641	1.80	4.70	0.31	6.442	2.28	0.20	3
SZ Aql	0.015	6559	2.00	6.00	0.13	6.421	2.32	0.13	6
SZ Aql	0.402	5147	1.10	3.85	0.25	6.421	2.35	0.14	6
SZ Cas	0.694	6157	1.60	4.30	0.02	9.832	2.50	0.20	5
SZ Cyg	0.293	5109	1.30	3.90	0.06	8.059	2.27	0.15	6
SZ Tau	0.296	6037	2.20	3.60	0.08	8.394	2.45	0.13	6
SZ Tau	0.426	5867	2.00	3.30	0.08	8.394	2.48	0.13	6
T Ant	0.173	6265	2.10	4.40	-0.24	8.384	2.14	0.12	2
T Cru	0.958	5940	2.20	5.10	0.09	7.546	2.25	0.13	3

Table 3 – *continued*

Star	phase	T _{eff} , K	log <i>g</i>	V _t , km s ⁻¹	[Fe/H]	R _G , (kpc)	log $\epsilon(\text{Ba})_{\text{NLTE}}$	$\sigma(\text{Ba})$	N lines
T Mon	0.562	4853	0.80	4.20	0.21	9.150	2.43	0.13	3
T Mon	0.600	4828	1.10	4.70	0.11	9.150	2.40	0.14	3
T Vel	0.827	5692	2.00	4.80	-0.02	8.054	2.26	0.15	3
T Vul	0.201	6077	2.00	3.55	0.02	7.760	2.35	0.18	6
T Vul	0.302	5899	2.00	3.30	0.03	7.760	2.43	0.17	6
TT Aql	0.457	5080	1.10	3.60	0.12	7.099	2.37	0.13	6
TT Aql	0.920	5630	1.60	5.10	0.09	7.099	2.37	0.14	6
TW CMa	0.059	6142	1.80	3.90	-0.18	9.764	2.37	0.20	2
TW Mon	0.167	5770	1.70	4.00	-0.24	13.608	2.38	0.13	3
TW Nor	0.094	5979	2.00	5.60	0.28	5.843	2.25	0.15	3
TX Cyg	0.936	6054	2.00	5.60	0.08	7.869	2.20	0.15	6
TX Del	0.005	6217	1.80	6.00	0.24	6.820	2.11	0.15	3
TX Mon	0.122	5871	1.80	4.90	-0.14	11.742	2.05	0.18	3
TZ Mon	0.817	5008	2.20	1.50	-0.03	11.439	2.29	0.13	3
TZ Mus	0.024	6348	2.10	4.60	-0.01	7.063	2.17	0.15	3
U Car	0.968	4934	0.80	5.80	0.01	7.537	2.27	0.15	3
U Nor	0.476	5426	1.40	3.60	0.15	6.815	2.33	0.10	3
U Vul	0.290	5965	1.85	4.10	0.13	7.584	2.43	0.13	6
U Vul	0.415	5655	1.75	4.00	0.10	7.584	2.43	0.14	6
UU Mus	0.041	6175	1.80	5.40	0.05	7.054	2.34	0.15	3
UW Car	0.035	6618	2.10	4.30	-0.06	7.617	2.05	0.12	3
UX Car	0.902	6442	2.60	4.70	0.02	7.663	2.19	0.12	3
UY Car	0.946	6376	2.40	5.70	0.03	7.548	2.05	0.15	3
UY Mon	0.674	6181	2.20	2.70	-0.08	10.085	2.47	0.18	2
UZ Car	0.044	6079	2.00	4.30	0.07	7.544	2.31	0.15	2
UZ Sct	0.455	5127	1.50	3.30	0.33	5.125	2.69	0.15	3
V Car	0.889	5906	2.10	5.20	0.01	7.877	2.22	0.12	2
V Cen	0.236	5705	2.10	3.90	0.01	7.426	2.15	0.12	3
V Cen	0.781	5616	1.80	4.80	0.01	7.426	1.95	0.12	3
V Cen	0.952	6427	2.30	4.60	0.01	7.426	2.15	0.13	3
V Lac	0.098	6470	1.90	3.60	-0.05	8.485	2.40	0.18	5
V Vel	0.043	6364	2.10	5.00	-0.23	7.849	2.00	0.13	3
V335 Aur	0.622	5750	2.20	3.50	-0.27	9.193	2.28	0.20	1
V339 Cen	0.142	5923	2.00	5.30	0.04	6.774	2.12	0.13	3
V340 Ara	0.167	5472	1.50	4.00	0.31	4.344	2.30	0.15	3
V340 Nor	0.193	5595	1.75	4.50	0.08	6.306	2.15	0.13	3
V340 Nor	0.430	5733	2.00	5.30	0.08	6.306	2.17	0.14	3
V350 Sgr	0.468	5557	1.90	3.70	0.15	7.065	2.34	0.15	6
V351 Cep	0.301	6005	2.10	3.30	0.03	8.313	2.27	0.18	3
V351 Cep	0.425	5944	2.50	4.30	0.03	8.313	2.21	0.18	2
V367 Sct		5891	2.10	4.25	-0.01	6.431	2.05	0.20	3
V378 Cen	0.131	6184	2.00	4.70	-0.02	7.054	2.35	0.13	3
V379 Cas	0.515	5943	2.00	3.50	0.04	8.592	2.50	0.15	6
V379 Cas	0.740	5969	2.00	3.50	0.01	8.592	2.50	0.14	6
V381 Cen	0.896	6224	2.30	5.10	0.02	7.236	2.20	0.13	3
V386 Cyg	0.961	6284	2.20	4.60	-0.04	7.888	2.27	0.15	6
V397 Car	0.903	6036	2.30	4.80	0.03	7.674	2.16	0.13	3
V402 Cyg	0.514	5518	1.55	3.70	-0.06	7.600	2.27	0.18	6
V419 Cen	0.905	6276	2.10	5.60	0.07	7.411	2.27	0.13	3
V440 Per	0.275	6048	2.20	4.80	-0.02	8.478	2.43	0.18	6
V440 Per	0.807	6041	2.00	4.80	-0.02	8.478	2.43	0.17	6
V465 Mon	0.373	6088	2.30	3.70	-0.04	10.088	2.45	0.18	6
V473 Lyr	0.559	6113	2.60	4.50	-0.06	7.726	2.35	0.15	3
V473 Lyr	0.793	6163	2.45	4.20	-0.06	7.726	2.45	0.16	3
V482 Sco	0.113	6129	2.20	4.00	0.07	6.945	2.31	0.13	3
V495 Mon	0.622	5591	1.60	4.00	-0.26	12.105	2.35	0.18	3
V496 Aql	0.043	5841	1.70	4.00	0.06	6.884	2.35	0.15	6
V496 Aql	0.910	5822	1.70	4.25	0.03	6.884	2.35	0.16	6
V496 Cen	0.025	6194	2.15	3.80	0.00	7.059	2.32	0.15	3
V500 Sco	0.051	5999	1.80	4.30	0.06	6.530	2.36	0.15	6
V500 Sco	0.340	5356	1.25	3.60	0.02	6.530	2.33	0.16	6
V504 Mon	0.714	6370	2.00	3.50	-0.31	10.676	2.13	0.13	3
V508 Mon	0.742	5566	1.60	4.00	-0.25	10.710	2.05	0.15	3
V510 Mon	0.232	5842	1.40	3.80	-0.19	12.956	2.48	0.15	3

Table 3 – *continued*

Star	phase	T _{eff} , K	log <i>g</i>	V _t , km s ⁻¹	[Fe/H]	R _G , (kpc)	log $\epsilon(\text{Ba})_{\text{NLTE}}$	$\sigma(\text{Ba})$	N lines
V526 Mon	0.674	6464	2.40	3.50		9.325	2.52	0.20	3
V532 Cyg	0.599	5960	2.00	3.10	0.08	7.981	2.47	0.15	6
V600 Aql	0.457	5604	1.70	4.00	-0.02	6.831	2.30	0.15	6
V636 Cas	0.151	5562	1.50	4.10	0.07	8.337	2.33	0.15	6
V636 Cas	0.270	5473	1.50	3.80	0.06	8.337	2.39	0.15	6
V636 Sco	0.969	5348	1.60	4.30	0.07	7.148	2.01	0.15	3
V659 Cen	0.856	6067	2.20	5.40	0.07	7.447	2.17	0.15	3
V733 Aql	0.699	5435	1.70	4.70	-0.01	6.187	2.02	0.15	5
V737 Cen	0.967	5865	2.00	4.50	0.13	7.335	2.45	0.13	3
V924 Cyg	0.702	5910	1.80	5.00	-0.09	7.529	2.10	0.20	3
V950 Sco	0.126	6322	2.20	4.20	0.11	7.099	2.22	0.13	3
V1154 Cyg	0.120	5840	1.80	4.10	-0.12	7.704	2.37	0.15	6
V1334 Cyg	0.253	6203	2.10	3.50	0.03	7.856	2.30	0.15	6
V1334 Cyg	0.295	6203	2.10	3.40	0.06	7.856	2.30	0.18	6
V1726 Cyg	0.109	6349	2.20	5.20	-0.02	8.177	2.14	0.20	3
VW Cru	0.175	5880	2.10	4.40	0.10	7.275	2.23	0.13	3
VW Pup	0.617	5586	1.90	4.60	-0.19	10.340	2.05	0.15	3
VX Cyg	0.411	5015	0.80	3.70	0.10	8.064	2.49	0.18	6
VX Per	0.709	5999	1.80	4.20	-0.03	9.627	2.52	0.20	6
VX Per	0.800	5992	1.80	4.20	-0.04	9.627	2.52	0.18	6
VX Pup	0.813	6159	2.50	3.50	-0.13	8.638	2.30	0.20	2
VY Car	0.169	4895	1.60	5.20	0.26	7.582	2.64	0.20	3
VY Cyg	0.370	5743	1.80	4.10	-0.02	7.885	2.27	0.15	6
VY Sgr	0.394	5144	1.25	3.30	0.26	5.584	2.50	0.15	3
VZ Cma	0.777	6542	2.50	3.60	-0.06	8.753	2.57	0.20	2
VZ Cyg	0.365	5670	1.80	3.30	-0.07	8.132	2.52	0.18	6
VZ Pup	0.980	6070	2.20	4.70	-0.16	10.404	2.25	0.19	3
W Gem	0.029	6416	2.25	5.00	-0.02	8.776	2.30	0.13	6
W Gem	0.136	6032	1.85	4.05	-0.01	8.776	2.35	0.14	6
W Gem	0.524	5475	1.70	3.90	-0.01	8.776	2.39	0.13	6
W Sgr	0.302	5927	1.85	3.70	0.04	7.512	2.40	0.15	6
W Sgr	0.462	5535	1.70	3.80	0.03	7.512	2.40	0.14	6
WW Car	0.852	5858	2.10	5.30	-0.07	7.515	1.87	0.13	3
WW Mon	0.750	6166	2.20	5.10	-0.29	12.943	2.30	0.15	3
WW Pup	0.722	5550	1.60	4.20	-0.18	10.068	2.07	0.15	3
WZ Car	0.009	5770	1.80	6.80	0.03	7.573	2.17	0.15	3
WZ Sgr	0.335	5077	1.10	3.80	0.20	5.964	2.40	0.15	3
WZ Sgr	0.942	6130	1.85	5.70	0.10	5.964	2.40	0.15	3
X Cru	0.125	5948	2.00	4.20	0.14	7.201	2.32	0.13	3
X Lac	0.328	5890	1.85	3.30	-0.01	8.477	2.42	0.18	5
X Pup	0.175	5848	1.30	5.00	-0.01	9.730	2.25	0.15	6
X Pup	0.213	5654	1.10	4.40	0.01	9.730	2.32	0.16	6
X Vul	0.062	6260	2.00	4.20	0.13	7.532	2.17	0.15	6
X Vul	0.220	5870	1.90	4.25	0.12	7.532	2.12	0.15	6
XX Car	0.692	5942	1.60	4.50	0.11	7.382	2.29	0.13	3
XX Cen	0.116	5953	2.00	5.00	0.16	6.997	2.40	0.13	3
XX Mon	0.704	5533	1.70	4.20	-0.18	11.946	2.20	0.15	3
XX Sgr	0.584	5557	1.60	3.20	0.05	6.632	2.53	0.18	6
XX Vel	0.011	6521	2.20	4.90	-0.05	7.708	2.10	0.13	3
XY Car	0.242	5738	1.70	4.60	0.04	7.356	2.07	0.13	3
XY Cas	0.603	5542	1.50	3.80	0.02	8.979	2.28	0.15	5
XZ Car	0.072	6170	2.10	5.70	0.14	7.414	2.32	0.15	1
Y Lac	0.858	6006	1.70	4.45	-0.08	8.419	2.17	0.18	6
Y Lac	0.936	6330	2.00	4.00	-0.10	8.419	2.17	0.17	6
Y Sgr	0.319	5733	1.65	3.80	0.11	7.425	2.43	0.18	6
Y Sgr	0.427	5605	1.60	3.70	0.04	7.425	2.45	0.18	6
YZ Car	0.860	5655	1.60	6.50	0.02	7.629	2.12	0.13	3
YZ Sgr	0.249	5507	1.40	3.65	0.06	6.799	2.24	0.15	6
YZ Sgr	0.775	5913	1.90	4.80	0.08	6.799	2.27	0.15	6
Z Lac	0.204	5722	1.50	3.80	0.05	8.564	2.37	0.15	6
Z Lac	0.930	5899	1.70	4.30	0.01	8.564	2.37	0.15	6